

Highly Unidirectional Emission and Ultralow-Threshold Lasing from On-Chip Ultrahigh-Q Microcavities

Xue-Feng Jiang, Yun-Feng Xiao,* Chang-Ling Zou, Lina He, Chun-Hua Dong, Bei-Bei Li, Yan Li, Fang-Wen Sun, Lan Yang, and Qihuang Gong*

Confinement and manipulation of photons using microcavities have triggered intense research interest for more than a decade.^[1] Prominent examples are whispering gallery mode (WGM) microcavities,^[2,3] which confine photons by means of continuous total internal reflection along a curved and smooth surface. The long photon lifetime (described by high Q factors), strong field confinement, and in-plane emission characteristics make them promising candidates for novel light sources^[4–9] and biochemical sensors with the ability of detecting few or even single nanoparticles.^[10,11] The principal disadvantage of circular WGM microcavities is their intrinsic isotropy of emission due to their rotational symmetry. In addition to the photonic structures consisting of two or more perfectly spherical microcavities,^[12] one of vital solutions is to use deformed microcavities by breaking the rotational symmetry,^[13–16] which can provide not only the directional emission but also the efficient and robust excitation of WGMs by a free-space optical beam.^[17–20] Deformed microcavities fabricated on a chip are particularly desired for high-density optoelectronic integration, but they suffer from low Q factors in experiments. The Q factors are typically around or even smaller than ten thousand^[21–27] limited by the large scattering losses from the involuntary surface roughness. The high Q factor is of great importance in fundamental studies and on-chip photonic applications. Here, with a pattern transfer technique and a reflow process ensuring a nearly atomic-scale microcavity surface, we demonstrate experimentally on-chip undoped silica deformed microcavities which support both nearly unidirectional emission and ultrahigh Q factors exceeding 100 million. Consequently, low-threshold, unidirectional microlasing in such a microcavity with Q factor about 3 million is realized by erbium doping and a convenient free-space excitation.

The deformed microcavities are fabricated from a 2- μm -thick layer of silicon dioxide on a silicon wafer. Combining a two-step dry etching process and a laser reflow process is employed for the first time to transfer patterns and achieve microcavities with designed shapes and ultra-smooth cavity surface. The process details are depicted in **Figure 1a**. First, we purposely design the mask patterns with minor modifications from the desired deformed toroidal boundaries $R(\varphi)$ by adding an extra 15 μm in the radius at all polar angles. Through optical lithography followed by buffered HF etching, deformed silica disks are created on the silicon wafer, which inherit the mask patterns well. Subsequently, the resulting silica disks are exposed to XeF_2 gas at 2.7 torr to etch the underneath silicon by about 15 μm . In this process, the silica disks keep their original shapes and also serve as etching masks for the silicon underneath; consequently a silicon pillar is formed under each disk. Owing to the isotropic dry etching of silicon, the underlying silicon pillars obtain the desired patterns. Then, the silica disks are reflowed by a CO_2 pulse laser irradiation, which melts the silica disks along the peripheries of the silicon pillars and causes the disks to collapse into toroids with ultra-smooth surfaces.^[28] Most importantly, the desired shapes are perfectly transferred from the silicon pillars back to the silica toroids as expected. Finally, a second XeF_2 dry etching process is applied to shrink the top diameter of the silicon pillars smaller than 10 μm . The small silicon pillar having a small overlap with the silica toroid is crucial to reduce the silica-to-silicon loss.

The deformed microcavity studied at present has the boundary defined in the polar coordinates (R, φ) as

$$R(\varphi) = \begin{cases} R_0 + \eta R_0 \sum_{i=2,3} a_i \cos^i \varphi \cos \phi \geq 0 \\ R_0 + \eta R_0 \sum_{i=2,3} b_i \cos^i \varphi \cos \phi < 0 \end{cases} \quad (1)$$

where η denotes the deformation parameter related to the aspect ratio of the shape; R_0 represents the size parameter. To achieve the highly unidirectional emission along 180° far-field direction (emitted at $\varphi \sim \pi/2$ and $3\pi/2$) from deformed silica microcavities, $a(b)_{2,3}$ are set as $a_2 = -0.1329$, $a_3 = 0.0948$, $b_2 = -0.0642$ and $b_3 = -0.0224$ (see Experimental Section and Supporting Information). After the sequenced pattern transfers from initial mask, to photoresist, to silica disk, to silicon pillar and finally back to silica toroid, the top view SEM image of a silica toroid and the close-up of the boundary shape are shown in **Figure 1b-c**, where the red dashed curve gives the ideal boundary with the designed parameter $\eta = 1$. It can be found that the microcavity inherits the pre-designed shape very well after going through several pattern transfers.

X.-F. Jiang, Prof. Y.-F. Xiao, B.-B. Li, Prof. Y. Li, Prof. Q. Gong
State Key Laboratory for Mesoscopic Physics
and Department of Physics
Peking University
Beijing 100871 P. R. China
E-mail: yfxiao@pku.edu.cn; qhgong@pku.edu.cn
C.-L. Zou, Dr. C.-H. Dong, Prof. F.-W. Sun
Key Lab of Quantum Information
University of Science and Technology of China
Hefei 230026, China
Dr. L. He, Prof. L. Yang
Department of Electrical and Systems Engineering
Washington University
St Louis, Missouri 63130, USA



DOI: 10.1002/adma.201201229

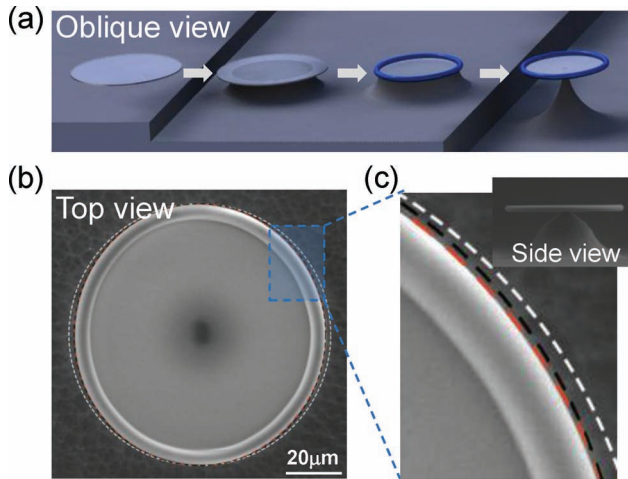


Figure 1. Fabrication of ultrahigh-Q deformed microcavities on a silicon chip. a) Flow diagram illustrating the fabrication process. From left to right: deformed silica disk, first-step undercut etching of the disk, CO₂ laser reflow and the second-step undercut etching of the deformed toroid. b,c) Top view scanning electron microscopy (SEM) image and its zoom-in of a toroid with $R_0 = 49 \mu\text{m}$ and $\eta = 1.0$. The red dashed curve indicates the designed boundary with $\eta = 1.0$. To facilitate comparison, black dashed curve shows boundary of an ellipse which has the same aspect ratio and major axis diameter with the designed boundary, and white dashed curve shows boundary of a circle which also has the same major axis diameter with the designed boundary. The inset shows a side view of the deformed toroid.

The microcavities are characterized in 1550 nm band with a free-space optical coupling system (see Supporting Information). The excitation laser is launched from a semiconductor tunable laser (TLB-6328, New Focus, with ultra-narrow linewidth of <300 kHz) and focused on the periphery of the microcavity by an objective (M Plan NIR 10 \times , Mitutoyo). The waist of the focused beam is about 3 μm . The emitted light from the microcavity is collected by the same or the other objective, then detected by a 125-MHz photoreceiver, and finally monitored by an oscilloscope. With this setup, the free-space transmission spectra are obtained by scanning the laser wavelength, and the scanning range and speed can be set by the laser controller, which have been calibrated by a high precision wavelength meter (WS7, Toptica, with absolute accuracy of 40 MHz). The microcavity is mounted on a rotational stage, which is placed on a translational stage (MDT630A, Thorlabs, with 20 nm resolution). A typical transmission spectrum for a microcavity is shown in Figure 2a. The incident beam is from 180° far-field direction and focused on the cavity edge at $\varphi \sim \pi/2$, and the collection is in the 0° far-field direction. It can be found that various high and low Q modes are efficiently coupled free from the strict phase matching condition, thanks to the dynamical tunneling between WGM-like

modes and neighboring chaotic modes.^[29,30] For comparison, the microcavity is also coupled to a tapered fiber,^[31] with the transmission spectrum shown in Figure 2b. It is clearly seen that all modes coupled to the taper can find their correspondences in Figure 2a, and the free-space coupling efficiently excites more modes. The free-space coupling efficiency relies on exact positioning of the incident free-space ray on the cavity edge with both high angular and translational resolution (see Supporting Information). In our experiment, the maximal efficiency ranges 15%–40% for cavity modes with different quality factors. For the measurement of a high-Q mode, for example the mode 1, a fine scan of the laser wavelength around the mode is implemented by applying a triangular-wave voltage to the piezoelectric transducer of the tunable laser, whose scanning frequency range and linearity have been calibrated by the high precision wavelength meter. The Q factor can also be obtained by a ring-down experiment (see Supporting Information). For the mode 1 with Q factor about 1.5×10^8 , the measured transmission spectra with both the free-space and taper couplings (Figure 2c-d) exhibit a doublet, originating from the mode coupling between a pair of counter-propagating WGMs induced by Rayleigh scattering.^[11] Double-Lorentzian fittings show that the resonant dips have the linewidths about 0.01 and 0.016 pm, together with a splitting of 0.033 pm for the free-space coupling; while for the taper coupling, the fitting linewidths are about 0.015 and 0.02 pm with a splitting of 0.032 pm. The additional linewidth in the latter case originates from the fiber taper coupling loss. In the experiment, electromagnetically induced transparency lineshapes (e.g., the modes 2-3) are usually observed in the transmission spectra with the free-space coupling, which may be attributed to coupling between a high-Q WGM and low-Q chaotic modes in the deformed microcavity.^[32,33]

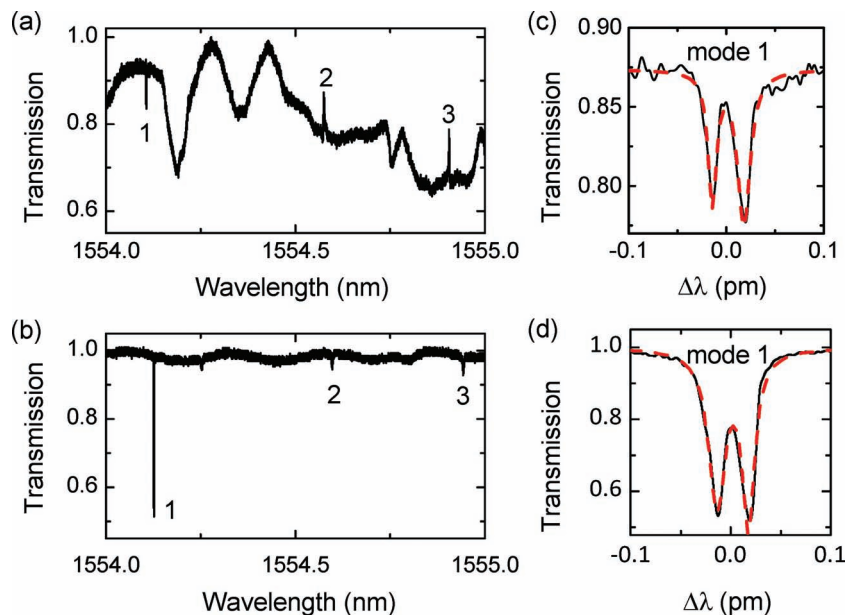


Figure 2. Transmission spectra obtained with the free-space excitation (a) and the fiber taper coupling (b). Numbers 1-3 marked in the plots indicate three corresponding high-Q optical modes. These modes show a minor red shift when coupled to the taper. c,d) Fine scanning for the mode 1 in (a) and (b). Here the red dashed curves show double-Lorentzian fittings.

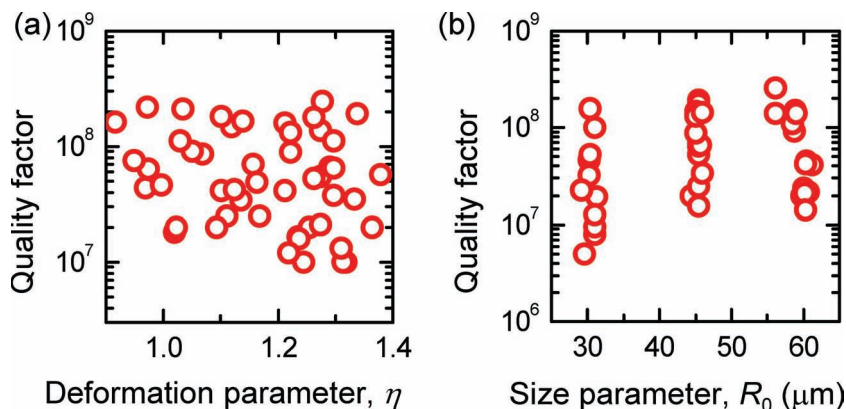


Figure 3. a,b) Experimental quality factors of various microcavities with different deformation and size parameters η and R_0 , respectively. In (a), $R_0 \sim 45 \mu\text{m}$ while in (b), $\eta \sim 1.0$.

In experiments, we fabricated various microcavities with different deformation and size parameters and measured the Q factors from the transmission spectra with the free-space optical coupling. The high-Q values can be derived by measuring the linewidths of the resonant dips in the transmission spectra (e.g., Figure 2c). As shown in Figure 3a,b, Q factors are typically higher than 10^7 , and the ultrahigh Q factor exceeding 10^8 can be routinely obtained. The reason for this ultrahigh experimental Q property is attributed to two factors. On one hand, the reflow process ensures a nearly atomic-scale surface of chip-based deformed microcavities, strongly suppressing the scattering loss from the surface roughness. On the other hand, the predicted Q factors in theory are ultrahigh over 10^8 for the microcavities with a large range of size and deformation parameters ($R_0 = 20 \mu\text{m}$ and $\eta < 1.5$) (see Supporting Information), and most importantly, the pre-designed shape can be perfectly transferred to the toroids. It is also noted that the Q values behave a non-systematic variation, which result from the cavity surface contaminations after fabrication in the lab environment, such as dust particles. In addition, a very small tendency for decreasing Q with increasing η is visible in Figure 3a, but the obtained highest quality factors keep almost unchanged.

Finally, to investigate the emission property of the deformed microcavities, we fabricated erbium-doped silica deformed microtoroids^[34] with the Er^{3+} ions concentration of $2 \times 10^{19} \text{ cm}^{-3}$. The gain medium in the microcavities may be efficiently excited using a free-space vertical focused laser beam^[35,36] where the pump laser is typically non-resonant with the cavity mode. Nevertheless, here we choose to excite the gain medium through a photonic channel (i.e., a high-Q cavity mode) which can provide a much

longer effective absorption length. Under the 1480 nm band resonant laser pumping (DL-100, Toptica) with the beam focusing on the periphery ($\varphi \sim \pi/2$), the active microcavity lases in 1550 nm band. The lasing spectrum is shown in Figure 4a. It is found that several WGMs can lase simultaneously under a strong pumping due to the broad gain profile. Here we focus on the lasing mode at 1560.15 nm. By applying a much weaker pump power ($< 50 \mu\text{W}$) with the free-space coupling efficiency of $\sim 35\%$, the microcavity can experience the single-mode operation (see Supporting Information). Figure 4b plots the lasing power at 1560.15 nm collected at direction versus the absorbed pumping power. The threshold for the absorbed power approaches as low as $2 \mu\text{W}$, further demon-

strating the ultrahigh Q property of the deformed microcavities. In the experiment, the quality factors of the erbium-doped samples are also measured for both the excitation and lasing modes, which are approximately 3×10^6 and 3.4×10^6 , respectively (see Supporting Information). These Q factors are limited by the

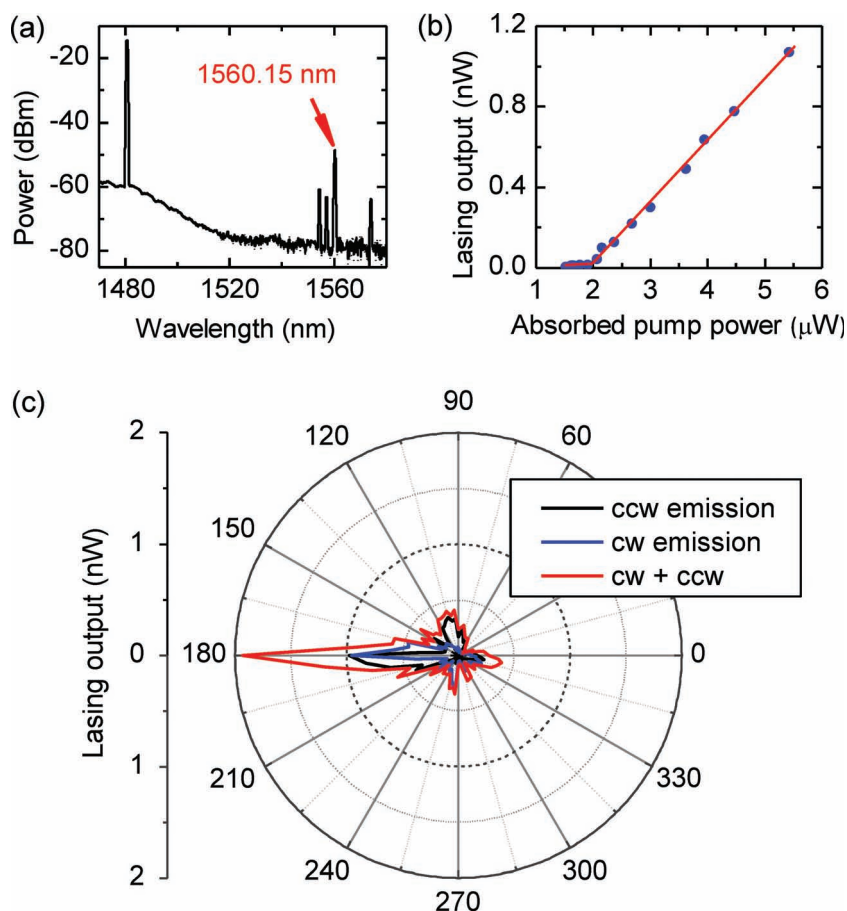


Figure 4. a) Lasing action in an Er^{3+} -doped deformed microcavity with $R_0 \sim 45 \mu\text{m}$ and $\eta \sim 1.03$, under the free-space pumping and collection. b) Threshold behavior for lasing at 1560.15 nm. c) Far-field emission patterns for the CW, CCW lasing at 1560.15 nm, and their sum, showing a highly unidirectional lasing emission along 180° direction.

erbium absorption, which can be directly calculated from the absorption cross-sections of erbium-doped glass and the doping concentration. Approximately, the absorption-related quality factors^[37] by erbium are 2×10^6 and 2.1×10^6 in the excitation and lasing bands, respectively. The slightly larger experimental Q factors may result from the deactivation of some erbium ions.

To directly characterize the emission property, we selectively collect the far-field emission from clockwise (CW) or counterclockwise (CCW) lasing, by introducing a spatial filter (pinhole) in the collection optical path (see Supporting Information). The resulting far-field patterns for 1560.15 nm lasing are shown in Figure 4c. It is found that both the CW and CCW lasing exhibit highly unidirectional emission with a narrow divergence angle smaller than 10 degrees.

In summary, we have demonstrated on-chip ultrahigh-Q microcavities with nearly unidirectional output characteristic. The recorded passive Q factors in such microcavities exceed 100 million in near infrared owing to near atomically smooth surface and special boundary design of the microcavities. Moreover, benefitting from near-perfect pattern transfers in the two-step dry etching and reflow processes, the microcavities possess pre-designed boundary which support highly intrinsic unidirectional emission even for a slight deformation. By doping erbium into the microcavity, lasing emission in 1550 nm band is observed under a convenient free-space optical pumping, with the threshold as low as $2 \mu\text{W}$. It is demonstrated that the well-controlled shape of the microcavity could allow us to achieve lasing emission along a single direction with a narrow divergence angle. We envision that this work opens up new possibilities for investigations of fundamental physics and applied photonics, such as ultralow threshold microlaser sources, strong coupling physics, and cavity optomechanics,^[38] by using a convenient free-space coupling in chip-based ultrahigh-Q microcavities. Further experiments include the realization of high-intensity, single-mode and unidirectional emission under both the optical and electric pumping.

Experimental Section

Mechanism of directional emission: Other than the circular microcavity, the deformed microcavity supports not only regular WGMs but also various chaotic modes. In wave optics, the regular WGMs can dynamically tunnel to neighboring chaotic modes, and the chaotic modes eventually refract out from the cavity at certain periphery areas. As a result, a directional emission pattern can be expected by designing the boundary shape of the deformed microcavity. In our design, the refractive escapes of the CCW propagating chaotic modes mainly occur at cavity periphery of $\varphi \sim \pi/2$, and the far-field direction of emission is along 180° . Symmetrically, the CW propagating chaotic modes leak out near the cavity periphery of $\varphi \sim 3\pi/2$ and show almost the same far-field emission direction.

Preparation of the Er^{3+} -doped deformed microcavities: In the active deformed microcavity experiments, erbium ion-doped silica film ($\sim 1.5 \mu\text{m}$) was first prepared on a silicon substrate using the standard sol-gel method. Dopant concentration was tailored by the amount of ions in the sol-gel solution. Then, the deformed active microcavities were created following the same process of the passive microcavities.

Supporting Information

Supporting Information is available from the Wiley Online Library or from the author.

Acknowledgements

This work was supported by the NSFC (Grants Nos. 11004003, 11023003, and 11121091). Y.F.X. was also supported by the Research Fund for the Doctoral Program of Higher Education (Grant No. 20090001120004). L. He and L. Yang acknowledge support from the U.S. National Science Foundation under Grant No. DMR0907467. Y.F.X. designed the experiments and wrote the paper. X.F.J., Y.F.X. C.H.D. and B.B.L. fabricated deformed microcavities and performed the measurements. L.H. and L.Y. prepared the active wafer for microlasing experiment. C.L.Z. and F.W.S. contributed to the theoretical work. Y.F.X. and C.L.Z. conceived the original idea. Y.F.X., Y.L. and Q.G. analyzed the data. All authors contributed to the discussion. Y.F.X. and Q.G. supervised and coordinated the project.

Received: March 25, 2012

Revised: May 16, 2012

Published online: August 13, 2012

- [1] K. J. Vahala, *Nature* **2003**, 424, 839.
- [2] S. L. McCall, A. F. J. Levi, R. E. Slusher, S. J. Pearton, R. A. Logan, *Appl. Phys. Lett.* **1992**, 60, 289.
- [3] H. M. Tzeng, K. F. Wall, M. B. Long, R. K. Chang, *Opt. Lett.* **1984**, 9, 499.
- [4] T. Carmon, K. J. Vahala, *Nat. Phys.* **2007**, 3, 430.
- [5] T. J. Kippenberg, R. Holzwarth, S. A. Diddams, *Science* **2011**, 332, 555.
- [6] J. U. Fürst, D. V. Strelakov, D. Elser, A. Aiello, U. L. Anderson, Ch. Marquardt, G. Leuchs, *Phys. Rev. Lett.* **2011**, 106, 113901.
- [7] P. T. Snee, Y. Chan, D. G. Nocera, M. G. Bawendi, *Adv. Mater.* **2005**, 17, 1131.
- [8] C. Rotschild, M. Tomes, H. Mendoza, T. L. Andrew, T. M. Swager, T. Carmon, M. A. Baldo, *Adv. Mater.* **2011**, 23, 3022.
- [9] J. Dai, C. X. Xu, X. W. Sun, *Adv. Mater.* **2011**, 23, 4115.
- [10] F. Vollmer, S. Arnold, D. Keng, *Proc. Natl. Acad. Sci. USA* **2008**, 105, 20701.
- [11] J. Zhu, S. K. Ozdemir, Y. F. Xiao, L. Li, L. He, D. R. Chen, L. Yang, *Nat. Photonics* **2010**, 4, 46.
- [12] M. Gerlach, Y. P. Rakovich, *Opt. Express* **2007**, 15, 17343.
- [13] A. F. J. Levi, R. E. Slusher, S. L. McCall, J. L. J. Glass, S. J. Pearton, R. Logan, *Appl. Phys. Lett.* **1993**, 62, 561.
- [14] J. U. Nöckel, A. D. Stone, *Nature* **1997**, 385, 45.
- [15] H. G. L. Schwefel, N. B. Rex, H. E. Tureci, R. K. Chang, A. D. Stone, T. Ben-Messaoud, J. Zyss, *J. Opt. Soc. Am. B* **2004**, 21, 923.
- [16] C. Gmachl, F. Capasso, E. E. Narimanov, J. U. Nöckel, A. D. Stone, J. Faist, D. L. Sivco, A. Y. Cho, *Science* **1998**, 280, 1556.
- [17] S. B. Lee, J. H. Lee, J. S. Chang, H. J. Moon, S. W. Kim, K. An, *Phys. Rev. Lett.* **2002**, 88, 033903.
- [18] S. Lacey, H. Wang, D. H. Foster, J. U. Nöckel, *Phys. Rev. Lett.* **2003**, 91, 033902.
- [19] Y. F. Xiao, C. H. Dong, C. L. Zou, Z. F. Han, L. Yang, G. C. Guo, *Opt. Lett.* **2009**, 34, 509.
- [20] J. Wiersig, M. Hentschel, *Phys. Rev. Lett.* **2008**, 100, 033901.
- [21] T. Harayama, T. Fukushima, S. Sunada, K. S. Ikeda, *Phys. Rev. Lett.* **2003**, 91, 073903.
- [22] G. D. Chern, H. E. Tureci, A. D. Stone, R. K. Chang, M. Kneissl, N. M. Johnson, *Appl. Phys. Lett.* **2003**, 83, 1710.

- [23] Q. J. Wang, C. Yan, N. Yu, J. Unterhinninghofen, J. Wiersig, C. Pflügl, L. Diehl, T. Edamura, M. Yamanishi, H. Kan, F. Capasso, *Proc. Natl. Acad. Sci. USA* **2010**, *107*, 22407.
- [24] Q. H. Song, L. Ge, S. D. Stone, H. Cao, J. Wiersig, J. B. Shim, J. Unterhinninghofen, W. Fang, G. S. Solomon, *Phys. Rev. Lett.* **2010**, *105*, 103902.
- [25] S. Shinohara, T. Harayama, T. Fukushima, M. Hentschel, T. Sasaki, E. E. Narimanov, *Phys. Rev. Lett.* **2010**, *104*, 163902.
- [26] C. Yan, Q. J. Wang, L. Diehl, M. Hentschel, J. Wiersig, N. Yu, C. Pflügl, F. Capasso, M. A. Belkin, T. Edamura, M. Yamanishi, H. Kan, *Appl. Phys. Lett.* **2009**, *94*, 251101.
- [27] C. H. Yi, M. W. Kim, C. M. Kim, *Appl. Phys. Lett.* **2009**, *95*, 141107.
- [28] D. K. Armani, T. J. Kippenberg, S. M. Spillane, K. J. Vahala, *Nature* **2003**, *421*, 925.
- [29] J. Yang, S. B. Lee, S. Moon, S. Y. Lee, S. W. Kim, T. T. A. Dao, J. H. Lee, K. An, *Phys. Rev. Lett.* **2010**, *104*, 243601.
- [30] J. Yang, S. B. Lee, J. B. Shim, S. Moon, S. Y. Lee, S. W. Kim, J. H. Lee, K. An, *Appl. Phys. Lett.* **2008**, *93*, 061101.
- [31] J. C. Knight, G. Cheung, F. Jacques, T. A. Birks, *Opt. Lett.* **1997**, *22*, 1129.
- [32] D. D. Smith, H. Chang, K. A. Fuller, A. T. Rosenberger, R. W. Boyd, *Phys. Rev. A* **2004**, *69*, 063804.
- [33] B. B. Li, Y. F. Xiao, C. L. Zou, Y. C. Liu, X. F. Jiang, Y. L. Chen, Y. Li, Q. Gong, *Appl. Phys. Lett.* **2011**, *98*, 021116.
- [34] L. Yang, T. Carmon, B. Min, S. M. Spillane, K. J. Vahala, *Appl. Phys. Lett.* **2005**, *86*, 091114.
- [35] M. V. Artemyev, U. Woggon, *Appl. Phys. Lett.* **2000**, *76*, 1353.
- [36] N. Gaponik, Y. P. Rakovich, M. Gerlach, J. F. Donegan, D. Savateeva, A. L. Rogach, *Nanoscale. Res. Lett.* **2006**, *1*, 68.
- [37] M. L. Gorodetsky, A. A. Savchenkov, V. S. Ilchenko, *Opt. Lett.* **1996**, *21*, 453.
- [38] Y. S. Park, H. Wang, *Nat. Phys.* **2009**, *5*, 489.